Experiments on Real-Time 1-Gbps Packet Transmission Using QRM-MLD with ASESS in MIMO-OFDM Broadband Packet Radio Access

Hiroyuki Kawai, Noriyuki Maeda, Junichiro Kawamoto, Kenichi Higuchi, and Mamoru Sawahashi

IP Radio Network Development Department, NTT DoCoMo, Inc.
3-5 Hikari-no-oka Yokosuka-shi, Kanagawa-Ken, 239-8536 Japan

Abstract - **This paper presents experimental results on real-time packet transmission of greater than 1 Gbps using 4-by-4 multiple-input multiple-output multiplexing (MIMO) employing Maximum Likelihood Detection (MLD) with a decreased level of computational complexity in Orthogonal Frequency Division Multiplexing (OFDM) radio access. We apply our original algorithm called adaptive selection of surviving symbol replica candidates based on the maximum reliability (ASESS) in MLD employing QR decomposition and the M-algorithm(QRM-MLD) to reduce the extremely high level of computational complexity in the conventional MLD. The experimental results using multipath fading simulators are in good agreement with the computer simulation results, confirming the effectiveness of our original signal detection algorithm, channel estimation filter, and likelihood function generation for successive soft-decision Turbo decoding based on real-time hardware implementation. We further show that the extremely high-speed real-time packet transmission of greater than 1 Gbps in a 100-MHz channel bandwidth (i.e., 10 bits/second/Hz) is achieved at the average received signal energy per bit-to-background noise power spectrum density ratio (E_b/N_0) per receiver antenna of approximately 12 dB using 16QAM modulation and Turbo coding with the coding rate of 8/9 in 4-by-4 OFDM multiplexing.**

I. Introduction

For future mobile communication systems beyond the 3G system, an all packet-based highly-efficient radio access scheme is necessary with a short delay (i.e., low latency) and with high affinity to IP-based core networks. Among the requirements for radio access, the supportable data rate is the most directly related to providing customer services. In Recommendation ITU-R M.1645, the maximum data rate supported in the new mobile access scheme is defined as 100 Mbps and that in the new nomadic/local area wireless access scheme is greater than 1 Gbps [1]. Although two different target data rates in the respective radio environments are defined in the recommendation, our concept is to support these two data rate requirements using the same radio access, i.e., the same air interface by only changing the radio parameters [2]. This concept is motivated by the desire to achieve seamless support of various radio environments using one radio access network deployment at low cost. We presented field experimental results on the measured throughput of greater than 100 Mbps using Variable Spreading Factor (VSF)-Orthogonal Frequency and Code Division Multiplexing (OFCDM) transceivers employing a 100-MHz channel bandwidth in real propagation environments [3]. Furthermore, the effectiveness of key techniques relevant to packet access such as adaptive modulation and channel coding (AMC) and hybrid ARQ with packet combining for broadband radio access with a 100-MHz channel bandwidth was clarified, and the achievable radio throughput and TCP throughput as a function of the cell distance in cellular environments were reported.

In this paper, we present experimental results on real-time packet transmission of greater than 1 Gbps by 4-by-4 multiple-input multiple-output (MIMO) multiplexing [4], [5] using Maximum Likelihood Detection (MLD) with a decreased level of computational complexity in Orthogonal Frequency Division Multiplexing (OFDM) radio access. We consider that the main application environments of MIMO techniques are local areas where there is a high traffic demand in a small area such as a hotspot, a very small cell with high traffic density, and indoors. Thus, assuming the application to such local areas, we employ a high coding rate together with a spreading factor of one based on the proposed VSF concept. The radio parameters such as the carrier frequency, channel bandwidth, and sub-carrier spacing of the implemented MIMO transceivers are identical to those of the transceivers with which we previously attained the throughput of greater than 100 Mbps in field experiments according to our proposed radio access concept [3].

The features of the implemented MIMO multiplexing transceiver are as follows. First, our signal detection method is based on MLD [6] because the required average received signal energy per bit-to-noise power spectrum density ratio (E_b/N_0) using MLD, which satisfies the same packet error rate (or throughput), is much smaller than that using linear co-channel suppression filtering with the Minimum Mean Squared Error (MMSE) criterion or Vertical-Bell Laboratories layered space time (V-BLAST) method [7]. We applied our original algorithm called adaptive selection of surviving symbol replica candidates based on the maximum reliability (hereafter ASESS) [8] in MLD employing QR decomposition and the M-algorithm (hereafter QRM-MLD) [9] to reduce the extremely high level of computational complexity in the conventional MLD (hereafter Full MLD). Second, the maximum information bit rate (corresponding to the frequency efficiency) achieved by 4-by-4 MIMO multiplexing is greater than 1 Gbps (10 bits/second/Hz) associated with 16QAM data modulation and Turbo coding with the coding rate of R = 8/9. Third, we applied an accurate two-dimensional multi-slot and sub-carrier averaging (MSCA) channel estimation filter [10], because accurate channel estimation is essential for achieving accurate signal detection. Fourth, we used likelihood function generation suitable for QRM-MLD, which is required for successive soft-decision Turbo decoding [11]. The rest of the paper is organized as follows. We first explain the design concept of the implemented MIMO multiplexing transceiver in Section II. Next, Section III describes the configuration of the implemented transceiver. Then in Section IV, we present experimental results focusing on the key techniques in Section II, and finally present real-time 1-Gbps packet transmission using a 100-MHz channel bandwidth.

II. Design Concept of MIMO Multiplexing Transceiver with Maximum Data Rate of 1 Gbps

The implemented maximum 4-by-4 MIMO multiplexing transceiver employs Spread OFDM radio access with a 101.5-MHz channel bandwidth. In this section, we explain the design concept and features of the implemented MIMO multiplexing transceiver that achieves the peak throughput of 1 Gbps (i.e., frequency efficiency of 10 bits/second/Hz).

A. Signal Detection Using QRM-MLD with ASESS

In OFDM radio access, a large frequency diversity effect is obtained through interleaving over a wide transmission bandwidth, which takes advantage of channel coding in a frequency-selective (multipath) fading channel. Due to this large frequency diversity effect, Turbo coding even with a high coding rate is still very effective in repairing decoding errors. In addition, ARQ is essential to packet radio access. It was reported that Incremental redundancy, which is hybrid ARQ with packet combining, is very effective in conjunction with a high coding rate, since the resultant low coding rate originating from the packet combining of retransmitted packets that have a different puncturing pattern than the initial one yields a large coding gain.

Among signal detection algorithms such as MLD, MMSE, and V-BLAST, the achievable throughput derived by using MLD is superior [6]. In particular, when the coding rate is high, the degradation in the signal separation of decision-feedback data symbols in V-BLAST becomes large due to the propagation of signal detection errors. We previously showed that the required average received E_b/N_0 at the average packet error rate (PER) of 10^{-2} using MMSE or the V-BLAST method [7] is degraded by more than 10 dB compared to that of MLD. Thus, we consider that the coverage area provided by a high throughput in MMSE or the V-BLAT method in MIMO multiplexing is limited to a very small area in a cellular system that suffers from severe other-cell interference compared to MLD, although the computational complexity level of MMSE or V-BLAST is much lower than that of MLD (note that although we consider the main application area is a local area, interference from the surrounding cells is not zero). Therefore, our approach is based on MLD signal detection. To decrease the extremely high level of computational complexity of Full MLD, we apply QRM-MLD [9]. Furthermore, we apply ASESS [8] to QRM-MLD, which we recently proposed to decrease further the complexity level of QRM-MLD. Let S_m be the number of surviving symbol replica candidates at the m-th stage (m is an integer such that $1 \leq m \leq N_{Tx}$, N_{Tx} is the number of transmitter antenna branches) in QRM-MLD. We must calculate the branch metric represented as the squared Euclidian distance S_m x 16 times for the symbol replica candidates at each stage assuming 16QAM modulation. On the other hand, by applying ASESS, we only have to calculate branch metrics for S_m symbol replica candidates. As a result, by using ASESS, the computational complexity from the viewpoint of the number of real multiplications in signal detection processing can be reduced to approximately 1/6 and 1/1900 that of the original QRM-MLD and Full MLD, respectively [8].

B. Two-dimensional MSCA Channel Estimation Filter

It is well known that the accuracy of signal detection in MIMO multiplexing/diversity strongly depends on the accuracy of the channel estimation. In QRM-MLD, since the Hermitian transposition of unitary matrix Q generated from channel matrix H using QR decomposition is multiplied to the received signal vector, the orthogonality of the transmission signals, which leads to the improvement in the signal detection accuracy, is affected by the accuracy of the estimated channel matrix. Therefore, we employ a time-division multiplexing (TDM) based orthogonal pilot channel and a two-dimensional MSCA channel estimation filter [10], in which we use pilot symbols as much as possible in multiple time slots and sub-carriers. By mitigating the degradation in tracking due to fluctuations in the phase and amplitude suffering from frequency-selective fading, we coherently average instantaneous channel estimates over multiple slots and sub-carriers after

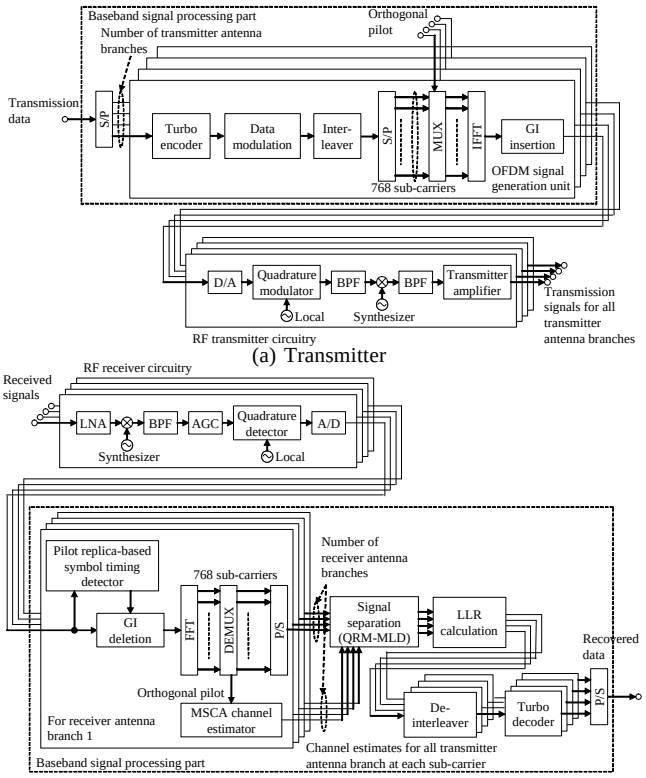

Figure 1. Configuration of implemented MIMO multiplexing transmitter and receiver.

weighting using the optimum-weighting factor.

C. Log Likelihood Ratio (LLR) Generation of A Posteriori Probability (APP) Suitable for QRM-MLD

We use Turbo coding and soft-decision decoding in the implemented MIMO multiplexing transceiver. Thus, the LLR of APP for each bit, $\hat{\Lambda}_{p,b}$, for the *b*-th bit from the *p*-th transmitter antenna branch is calculated from the accumulated branch metrics of the surviving symbol candidates at the last stage of the QRM-MLD with ASESS as

$$\hat{\Lambda}_{p,b} = \left(\sqrt{e_{\min,p,b,-1}} - \sqrt{e_{\min,p,b,1}}\right) \tag{1}$$

where $e_{\min,p,b,v}$ is the minimum accumulated branch metric among the surviving symbols for bit "*v*" for the *b*-th bit from the *p*-th transmitter antenna branch ($1 \le p \le N_{Tx}$, N_{Tx} is the number of transmitter antenna branches). It should be noted that the accumulated branch metrics representing both "1" and "-1" are needed for each bit to calculate the $\hat{\Lambda}_{p,b}$ value. Thus, assuming soft-decision Turbo decoding, there is a problem such that the LLR of the APP cannot be obtained when no surviving symbol candidates containing either bit "1" or "-1" remain. Therefore, we use the likelihood function generation method in [11] for bits when the surviving symbol replica candidates do not remain at the last stage in QRM-MLD.

D. TCP/IP Interface

The interface between the implemented MIMO multiplexing transceiver and the external application terminal adopts the Ether format. Thus, demonstration of high-speed data download and high-definition video transmission based on TCP/IP is possible.

III. Configuration of Implemented MIMO Multiplexing Transceiver

The implemented MIMO transmitter and receiver configurations are illustrated in Figs. 1(a) and 1(b), respectively, and they employ the major radio link parameters listed in Table I. The channel bandwidth and the number of sub-carriers of the OFDM signal are 101.5-MHz and 768, respectively (thus, the sub-carrier separation is 131.836 kHz). The length of the packet frame is 0.5 msec, which contains 54 OFDM symbols (see Fig. 2). In the base station (BS) transmitter (we focus on the downlink) binary information data bits are first serial-to-parallel converted to four streams corresponding to four transmitter antenna branches, and then encoded using Turbo coding with the coding rate of *R* with the constraint length of four bits. After 16QAM data modulation mapping, symbol interleaving is performed to randomize the burst errors due to frequency-selective fading in the frequency domain over 768 sub-carriers. The four pilot symbols used for channel estimation are time-multiplexed within a packet frame. Then, each encoded data sequence is converted into a multicarrier signal with 768 sub-carriers using the

Table I. Major Radio Link Parameters of Testbed

Radio access	VSF-Spread OFDM
Bandwidth	101. 5 MHz
Number of antenna branches	2 – 4 (Transmitter and receiver)
Number of sub-carriers	768 (131.836 kHz sub-carrier separation)
OFDM symbol duration	7.585 μsec + GI 1.674 μsec (1024 + 226 samples)
Spreading factor	1
Data modulation	16QAM
Channel coding / decoding	Turbo code (*R* = 1/2 - 8/9, *K* = 4) / Max-Log-MAP decoding
Signal separation	QRM-MLD with adaptive surviving symbol replica candidate selection method
OFDM symbol timing detection	Pilot symbol replica-based detection
Channel estimation	Orthogonal pilot channel-based MSCA channel estimation filter

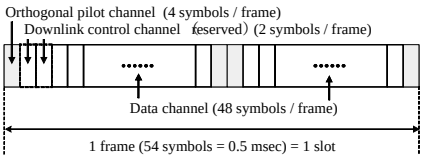

Figure 2. Packet frame format.

Inverse fast Fourier transform (IFFT). After conversion into baseband in-phase (I) and quadrature (Q) components by digital-to-analog (D/A) converters, quadrature-modulation is performed. Finally, the IF modulated signal is up-converted into the RF signal and amplified by the power amplifier where the center carrier frequency is 4.635 GHz.

At the mobile station (MS) receiver, the frequency down-converted IF signal is first linearly amplified by an automatic gain control (AGC) amplifier. The received spread signal is converted into baseband I and Q components by a quadrature detector. The I and Q signals are converted into digital format by the analog-to-digital (A/D) converters. The OFDM symbol timing is estimated by taking the maximum cross-correlation peak between the received baseband digital signal and a reference signal such as a pilot symbol (this symbol timing is updated every 0.5 msec). After the guard interval is removed, 768 parallel data sequences are demultiplexed by FFT processing from the multi-carrier signal with 768 sub-carriers. The channel gain of each packet frame at each sub-carrier is estimated using a MSCA filter as shown in Fig. 3 [10]. Let $d_{p,pilot}(b)$ be the received pilot symbol of the *b*-th symbol from the *p*-th transmitter antenna branch. Then, we derive the channel gain of the target time slot and sub-carrier by coherently averaging four pilot symbols belonging to the slot as

$$\hat{x}_{p,q,k}(n) = \frac{1}{4}\sum_{b=1}^{4} y_{q,k}(n,b) d^{*}_{p,pilot}(b) \tag{2}$$

where $y_{q,k}(n,b)$ represents the received signal after FFT processing of the *k*-th sub-carrier ($1 \le k \le N_{sub}$) of the *b*-th symbol ($1 \le b \le N_{symbol}$) for the *n*-th frame at the *q*-th branch ($1 \le q \le N_{Rx}$, N_{Rx} is the number of receiver antenna branches). The instantaneous channel gain of the *n*-th slot at the *k*-th sub-carrier, $x_{p,q,k}(n)$, is further weighted and coherently combined with the appropriate weights over ($2N_{Freq}$ +1) sub-carriers and $2N_{Time}$ slots with the *k*-th sub-carrier and the *n*-th slot as the center, respectively, as shown below.

$$\tilde{x}_{p,q,k}(n) = \frac{1}{\sum_{k'=-N_{Freq}}^{N_{Freq}} \sum_{n'=-(N_{Time}-1)}^{N_{Time}} a_{Freq,k'} a_{Time,n'}} \sum_{k'=-N_{Freq}}^{N_{Freq}} \sum_{n'=-(N_{Time}-1)}^{N_{Time}} a_{Freq,k'} a_{Time,n'} \hat{x}_{p,q,k+k'}(n+n') \tag{3}$$

where $a_{Freq,k'}$ and $a_{Time,n'}$ are the real-valued weighting factors for the (*k*+*k'*)-th sub-carrier and the (*n*+*n'*)-th slot. Here, we set N_{Freq} = 1 and N_{Time} = 1. Furthermore, we set $a_{Time,-1} = a_{Time,0} = a_{Time,1} = 1.0$. Factor $a_{Freq,k'}$ is set to one when *k'* = 0, otherwise it is assumed that $a_{Freq,+k'} = a_{Freq,-k'}$. Weights are determined such that the required average received E_b/N_0 is minimized based on the tradeoff relationship between the increase in the signal power and mitigation of the fluctuation of the channel gain due to fading as investigated in the subsequent section. Figure 4 illustrates the configuration of QRM-MLD using ASESS. From the estimated channel gain, we generate channel matrix $\hat{\mathbf{H}}_k(n)$. Let $\mathbf{Q}_k(n)$ be the unitary matrix with the size of N_{Rx} x N_{Tx}. In QRM-MLD, by performing QR decomposition for the estimate of the channel matrix as $\hat{\mathbf{H}}_k(n) = \mathbf{Q}_k(n)\mathbf{R}_k(n)$, the obtained matrix, $\mathbf{R}_k(n)$, becomes an upper triangular matrix with the size of N_{Tx} x N_{Tx}. By multiplying $\mathbf{Q}_k(n)^{\mathrm{H}}$ with the received signal in vector notation of the *k*-th sub-carrier, $\mathbf{Y}_k(n,b)$, the received signal in vector notation after nulling (i.e., orthogonalization), $\mathbf{Z}_k(n,b)$, is generated as

$$\mathbf{Z}_k(n,b) \equiv \mathbf{Q}_k(n)^{\mathrm{H}} \mathbf{Y}_k(n,b) = \mathbf{R}_k(n)\mathbf{d}_k(n,b) + \mathbf{n'}_k(n,b) \tag{4}$$

where $\mathbf{d}_k(n,b)$ is the transmission data in vector notation and $\mathbf{n'}_k(n,b)$ is a noise component multiplied by $\mathbf{Q}_k(n)^{\mathrm{H}}$. In QRM-MLD comprising stages corresponding to the number of transmitter branches, N_{Tx}, the symbol replicas with high reliability are successively selected stage-by-stage using $\mathbf{Z}_k(n,b)$ and $\mathbf{R}_k(n)$ based on the M-algorithm.

Figure 5 shows the configuration of the proposed QRM-MLD using ASESS. In the ASESS method, we calculate the squared Euclidian distance only for the minimum number of the remaining symbol replica candidates at each stage by taking advantage of the reliability information of the symbol replica candidates newly-added at each stage. The ASESS algorithm based on the maximum reliability comprises the following two steps at each stage in QRM-MLD [8].

Step 1: Symbol replica candidates newly-added at each stage are ranked for each

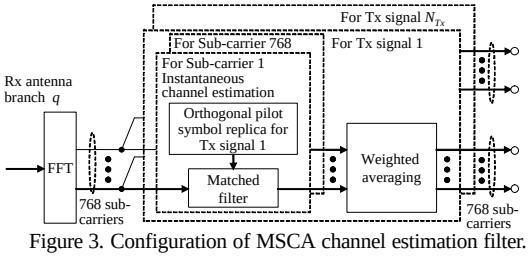

Figure 3. Configuration of MSCA channel estimation filter.

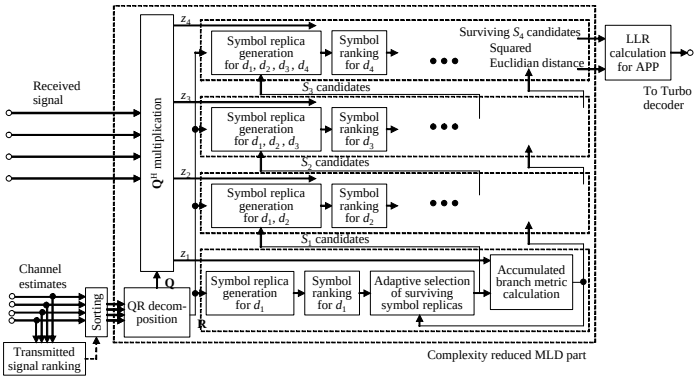

Figure 4. Configuration of QRM-MLD with ASSES.

surviving symbol replica candidate from the previous stage based on multiple quadrant detection.

Step 2: The surviving symbol replica candidates that pass to the next stage are selected using two sets of information, i.e., the "representative" accumulated branch metrics and the symbol ranking results using an iterative loop. We consider the operation in the m-th stage in QRM-MLD after ranking the 16-symbol replica candidates of the m-th transmitted signal for each surviving symbol replica candidate in the (m-1)-th stage based on the process.

(1) Let $E_{m-1,1}$, ..., $E_{m-1,S_{m-1}}$ be the accumulated branch metrics up to the (m-1)-th stage for the surviving symbol replica candidates. We set $E_{m-1,1}$, ..., $E_{m-1,S_{m-1}}$ to the initial representative accumulated branch metric at the m-th stage, $M_{m,1}$, ..., $M_{m,S_{m-1}}$ for each surviving symbol replica candidate. Furthermore, we set the symbol index after ranking the 16-symbol replica candidates for the m-th transmitted signal for each surviving symbol replica candidate in the (m-1)-th stage, $i_{m,1}$..$i_{m,S_{m-1}}$, to one. Also, iteration index, j, is set to one.

(2) The surviving symbol replica in the (m-1)-th stage, $\mathbf{c}_{m-1,\hat{x}}$, with the minimum representative accumulated branch metric, i.e., $\hat{x} = \arg\min_x M_{m,x}$, is selected.

(3) Symbol replica candidate $\mathbf{c}_{m-1,\hat{x}}$ with the $i_{m,\hat{x}}$-th ranked newly-added symbol replica candidate of the m-th transmitted signal is selected as the j-th surviving symbol replica candidate, $c_{m,j}$, for the next stage.

The accumulated branch metric at the m-th stage, $E_{m,j}$, for $c_{m,j}$ is calculated.

(4) $E_{m,j}$ is set to a new $M_{m,\hat{x}}$. Index $i_{m,\hat{x}}$ and parameter j are both increased by one.

The process from (2) to (5) is repeated until the number of surviving symbol replicas in the m-th stage becomes S_m (i.e., up to $j = S_m$).

Note that in the implemented MS receiver, the ASESS processing in QRM-MLD is implemented by cards in two shelves as shown in Fig. 6 using only commercial Field Programmable Gate Arrays (FPGAs) and Digital Signal Processors (DSPs). The size of the signal separation part would be approximately six times larger if the original QRM-MLD is applied.

We use likelihood function generation for bits when the surviving symbol replica candidates do not remain to the last stage in QRM-MLD as follows [11] (see Fig. 7). (a) The minimum accumulated squared Euclidian distance (i.e., accumulated branch metric) of each bit "1" and "-1" is derived as the likelihood function of each bit for the surviving symbol candidates. (b) For a bit that has both bits "1" and "-1" in the remaining symbol replica candidates in the last stage (let N_B be the number of bits, which has both bits "1" and "-1" in the remaining symbol replica candidates in the last stage), the larger likelihood function of the two bits, "1" or "-1," is selected. (c) The selected N_B larger likelihood functions are summed and the summation is normalized by N_B. (d) Finally, the averaged likelihood function calculated in Step (c) is multiplied by a factor of "X." The obtained likelihood function is used as obtained for the bit, which does not remain in the remaining symbol replica candidates in the last stage. Finally, the output LLR streams of QRM-MLD are parallel-to-serial-converted and soft-decision Turbo decoded by Max-Log-MAP decoding with eight iterations to recover the transmitted binary data.

IV. Experiment Setup

In the subsequent experiments in Section V, we set the number of transmitter and receiver antenna branches to be $N_{Tx} = N_{Rx} = 4$ except for the cases in Figs. 12 and 13 and N_{Tx} and N_{Rx} are parameterized in Figs. 12 and 13. Data modulation is assumed to be 16QAM except for Fig. 14. In the experiments, we employed 16 multipath adding simulators to simulate frequency-selective Rayleigh fading channels. A six-path channel is generated using multipath fading simulators where each

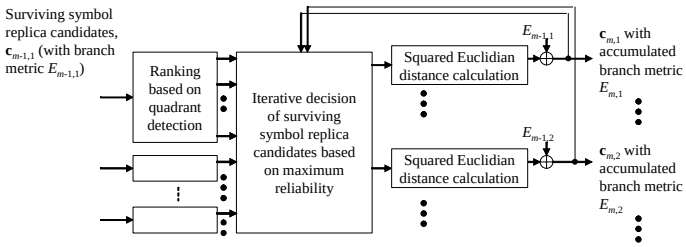

Figure 5. Configuration of m-th stage of ASSES in QRM-MLD.

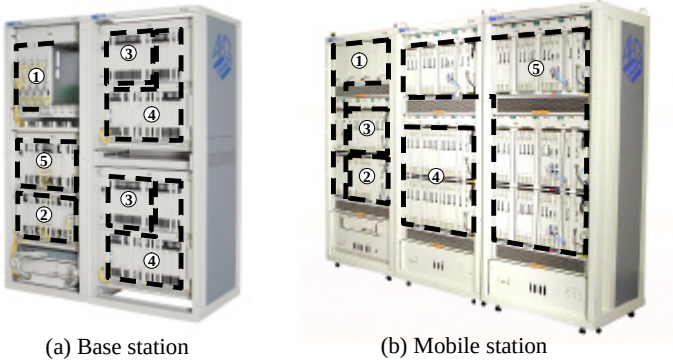

(a) Base station (b) Mobile station

① Power amplifier and transceiver part
② Transmitter baseband processing part
③ Synchronization and channel estimation part
④ Signal detection part (QRM-MLD based)
⑤ AMC, Channel decoding, Hybrid ARQ, and IP packet processing part (for 4 transmitted signals)

Figure 6. Views of implemented base station and mobile station transceivers.

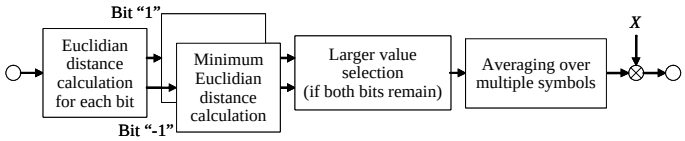

Figure 7. Likelihood function generation for bits when the surviving symbol replica candidates do not remain to the last stage in QRM-MLD.

path is independently Rayleigh-faded with the root mean squared (r.m.s.) delay spread, s, of 0.26 μsec, and where the average signal power is decreased by 2 dB in descending order from the first path. Furthermore, the fading maximum Doppler frequency is set to 20 Hz, which corresponds to the moving speed of approximately 4.3 km/h. The r.m.s. delay spread value of s = 0.26 μsec is from the field experimental results conducted in downtown Yokosuka with the BS-to-MS distance of approximately 1 km [3]. In the field experiments, we observed over 20 paths. However, based on the restrictions of the hardware multipath fading simulators, the number of paths was set to 6. We confirmed that there is no distinct difference between 6 paths and 20 paths from the viewpoint of frequency diversity, since there is no path with a long time delay that exceeds the guard interval duration [3]. We set the fading correlation among the transmitter and receiver antenna branches to be zero. The output of the multipath fading simulators is combined and additive white Gaussian noise is added at each receiver antenna branch of the MIMO receiver.

V. Experimental Results

A. Effect of MSCA Channel Estimation Filter

We first investigate the measured average PER performance employing QRM-MLD with ASESS focusing on the two-dimensional MSCA channel estimation filter. Figs. 8(a) and 8(b) show the average PER performance with the weighting factors of the MSCA channel estimation filter $\alpha_{Freq,+1}$ as a parameter, as a function of the average received E_b/N_0 per receiver antenna branch. Figures 8(a) and 8(b) indicate the PER performance with R = 1/2 and 8/9 (the corresponding information bit rate is 500 Mbps and 1 Gbps), respectively. The computer simulation results are also given for comparison. In the simulation, the quantization by A/D converters is not performed unlike in the implemented transceiver. The number of surviving symbol replica candidates is set to $S_{2\text{-}4}$ = 16. Furthermore, in Figs. 8(a), 8(b), and the subsequent Fig. 9, the Euclidian distance is employed for LLR calculation at the output of the QRM-MLD with ASESS and the weighting factor of likelihood function for the bits, which does not exist at the last stage, is set to X = 1.5. Figure 8(a) clearly shows that the loss in the required average received E_b/N_0 at the average PER of 10^{-2} of the experiments from the simulation results is only within 1.0 dB for the case with R = 1/2, indicating good agreement with the simulation results. Moreover, Fig. 8(b) shows that the degradation is increased to approximately 2 dB when R is 8/9. The reason why the degradation of the required average received E_b/N_0 for R = 8/9 is increased is caused mainly by the quantization of 12-bit A/D converters since the required average received E_b/N_0 becomes high. Figure 8(b) shows that in the experiments, the required average received E_b/N_0 employing the MSCA channel estimation filter using $\alpha_{Freq,+1}$ = 0.2

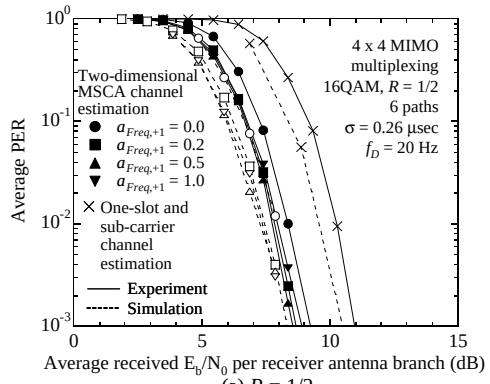

(a) R = 1/2

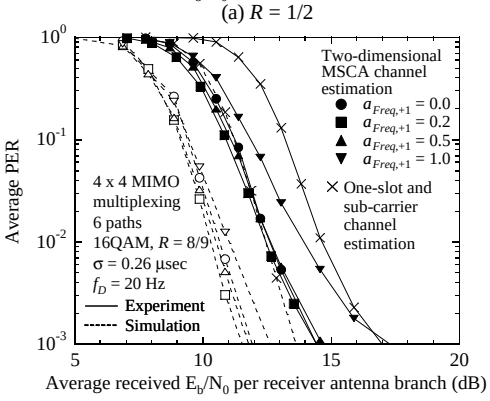

(b) R = 8/9

Figure 8. Average PER performance with aFreq in MSCA as a parameter.

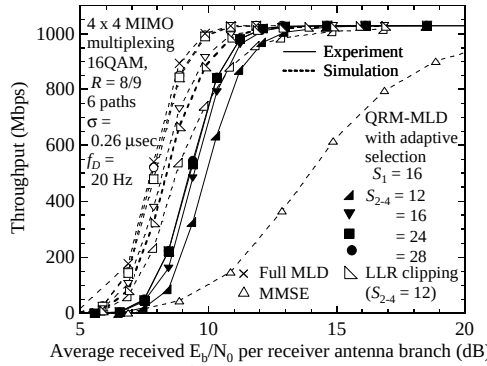

Figure 9. Throughput performance with Sm in ASSES as a parameter.

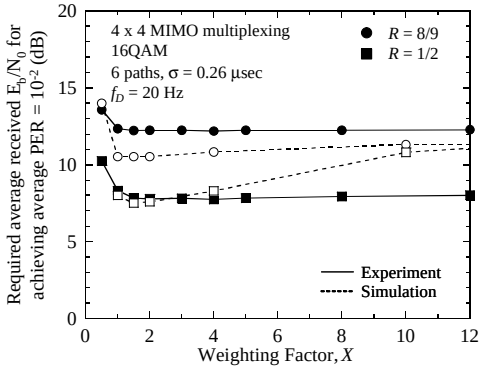

Figure 10. Average received E_b/N_0 required for achieving average PER of 10^{-2} as a function of weighting factor, X, for calculating LLR.

at the average PER of 10^{-2} is decreased by approximately 2 dB compared to that of the channel estimation using only four pilot symbols within the target slot. This is because the impact of background noise is reduced by averaging using more pilot symbols, which takes advantage of the fading correlation between adjacent subcarriers. Thus, we also show the effectiveness of the MSCA channel estimation filter in the experiments based on a real hardware implementation.

B. Effect of ASESS

Next, the measured throughput performance using the QRM-MLD with ASESS is plotted in Figs. 9 as a function of the average received E_b/N_0 with R = 8/9. The number of surviving symbol replica candidates in Stage 1 is set to S_1 = 16 and those of the other stages, $S_{2-4,}$ are parameterized. The computer simulation results of ASESS in QRM-MLD and those of the original QRM-MLD, Full MLD, and MMSE are given in the figure for comparison. Figures 9 clearly show that according to the increase in the S_{2-4} value, the achieved throughput is increased, since false discard probability of the correct symbol replica candidates is reduced in QRM-MLD with ASESS. These experimental results agree well with the simulation results similar to those in Fig. 8. When the number of surviving symbol replica candidates is large, i.e., S_{2-4} is greater than 16, the loss in the required average received E_b/N_0 in the experimental results from the simulation results becomes approximately 2.0 dB. These results coincide with the PER performance in Fig. 8. However, we find that when the S_{2-4} value is small such as 12, the experimental results become more favorable than the simulation results. Here, as mentioned previously, the simulation results do not perform quantization using A/D converters. The amplitude component is not clipped at all. Thus, we added to Fig. 9 simulation results for 12-bit quantization represented as a bold dotted line. The simulation results with quantization are improved by 1-2 dB in the required average received E_b/N_0 compared to the experimental results, indicating reasonable results the same as that for S_{2-4} of more than 16. This reason is explained as follows. The situation occurs such that both bits "1" and "-1" do not exist in the remaining symbol replica candidates in the last stage for the QRM-MLD. In this case, although we calculate LLR based on the proposed method in Section II, a higher likelihood function value for the bit that does not exist than that for the existing bits degrades the achievable performance due to the decoding error in soft-decision Turbo decoding. Therefore, by using the clipping from the quantization, an excessively high LLR for the non-existing bits is limited [11].

Furthermore, Fig. 9 clearly shows that the QRM-MLD with ASESS using S_{2-4} = 28 achieves the throughput of 1 Gbps at the average received E_b/N_0 of approximately 12.0 dB in the real-time hardware implementation. The figure also shows that by comparing the simulation results the loss in the required average received E_b/N_0 of the QRM-MLD from that of the Full MLD is suppressed to within 0.5 dB and the required value can be decreased by more than 10 dB compared to that of MMSE. The main impairment to the experimental results compared to the simulations is the quantization noise originating from the A/D converters. Thus, it is considered that the degradation similarly affects QRM-MLD with ASESS, the Full MLD, and MMSE. Accordingly, we anticipate that the same relative throughput performance levels can be obtained in real-time hardware implementations with the degradation of 1-2 dB in the required average received E_b/N_0 from the simulation results.

C. LLR Generation of APP for Soft Decision Turbo Decoding

Figure 10 shows the measured average received E_b/N_0 at the average PER of 10^{-2} as a function of the weighting factor, X, for calculating the LLR. We used the Euclidian distance, i.e., root of the squares of the Euclidian distance as a branch metric, although the squared value is generally used [11]. We set R = 1/2 and 8/9. The figure shows that the required average received E_b/N_0 is first decreased by reducing the X value to approximately 1.0. This is because by lowing the likelihood (i.e., large LLR value), the error in the LLR of APP for the bit, which does not exist among the surviving symbol candidates at the last stage of QRM-MLD, is mitigated. However, when we increase the X value beyond approximately 4.0, the required average received E_b/N_0 is slightly increased. This is because the achievable performance approaches that for hard-decision Turbo decoding. Compared to the simulation results, the degradation in the required average received E_b/N_0 of the experimental results becomes small when the X value is greater than approximately 4.0. This is because the calculated LLR information for the non-existing bit is limited by the quantization, leading to a reduction in the error of LLR in the succeeding Turbo decoder. Thus, we conclude that the required average received E_b/N_0 is decreased most in the X value range of approximately 1.0 to 4.0 both for R = 1/2 and 8/9.

Figure 11 shows the average PER performance as a function of the average received E_b/N_0 using two types of LLR calculation methods: squared Euclidian distance and direct Euclidian distance (i.e., root of the squared Euclidian distance, as shown in Eq. (1)) in QRM-MLD with ASESS. We set X = 1.5 based on the results in Fig. 10. The figure shows that the required average received E_b/N_0 at the average PER of 10^{-2} employing the Euclidian distance is reduced by approximately 1.0 dB compared to that for the squared Euclidian distance. This is because the likelihood function based on the Euclidian distance can mitigate the estimation errors in the likelihood function of the bits that do not remain among the surviving symbol candidates in the last stage compared to that for the squared Euclidian distance. Thus, in the subsequent experiments, we use the Euclidian distance to calculate the LLR of APP.

D. Effect of Number of Transmitter/Received Branches

Figure 12 shows the measured average PER performance of QRM-MLD with ASESS as a function of the average received E_b/N_0 with the number of receiver antenna branches of N_{Rx} = 4 and with the number of transmitter antenna branches, N_{Tx}, as a parameter from 1 to 4. When the N_{Tx} value is 1, 2, 3, and 4, the information bit rate becomes 257, 514, 771, and 1028 Mbps for the coding rate of R = 8/9. The computer simulation results are also given for comparison. Figure 12 shows that according to the increase in the N_{Tx} value, the loss in the required average received E_b/N_0 at the average PER of 10^{-2} in the experimental results compared to that in the simulation results is increased. However, even with N_{Tx} = 4 (4-by-4 MIMO multiplexing), the loss in the required average received E_b/N_0 is within 2 dB. The figure also shows that the required average received E_b/N_0 at the

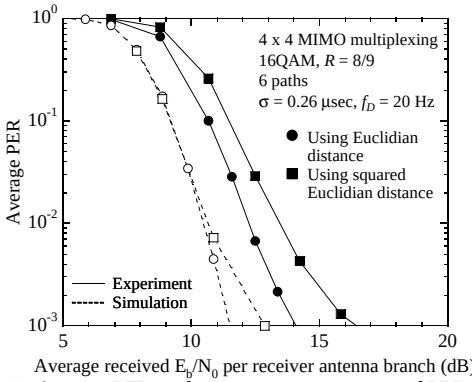

Figure 11. Average PER performance using two types of LLR calculation.

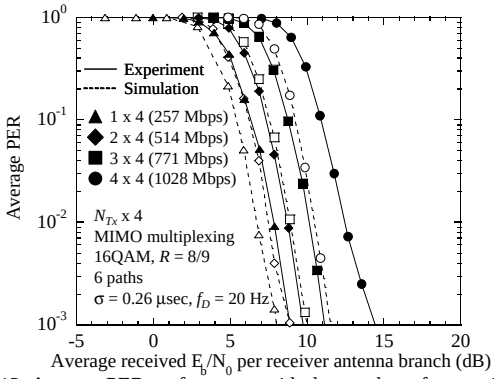

Figure 12. Average PER performance with the number of transmitter antenna branches, N_{Tx}, as a parameter.

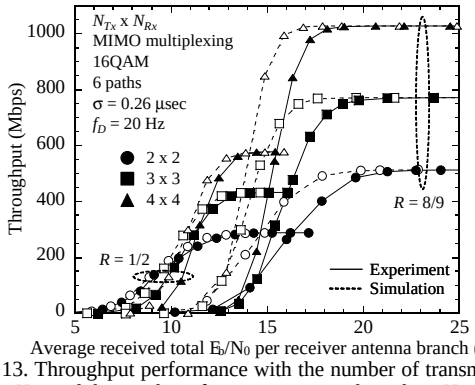

Figure 13. Throughput performance with the number of transmitter antenna branches, N_{Tx}, and the number of receiver antenna branches, N_{Rx}, as parameters.

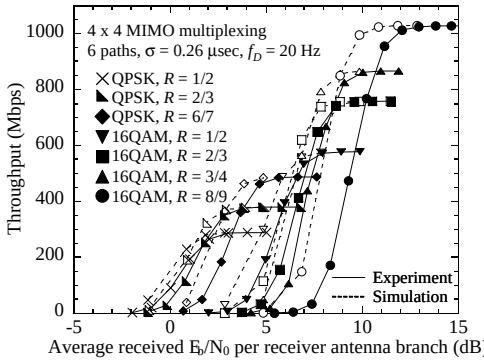

Figure 14. Throughput performance for various sets of modulation and coding rate.

average PER of 10^{-2} with N_{Tx} = 4 is increased by approximately 4.5 dB compared to that of N_{Tx} = 1. Note that since the information bit rate with N_{Tx} = 1 is 257 Mbps, the results with N_{Tx} = 1 indicate that the data rate of 1.028 Gbps is achieved using a four fold larger channel bandwidth of the implemented transceiver (i.e., 400 MHz). Therefore, we understand that by using 4-by-4 MIMO multiplexing employing QRM-MLD with ASESS, the information bit rate of 1 Gbps is achieved by 1/4 the channel bandwidth in the case with N_{Tx} = 1 by allowing the increase in the required average received E_b/N_0 of approximately 4.5 dB.

Figure 13 indicates the measured throughput of QRM-MLD with ASESS when the combination of (N_{Tx}, N_{Rx}) is changed from two to four as a function of the average received total E_b/N_0 per receiver branch. Here, the total E_b denotes the signal energy per bit of the entire transmission signal from the N_{Tx} antenna branches, since we assume a constant total transmission power irrespective of the N_{Tx} value for fair comparison. The figure shows that when the average received total E_b/N_0 is less than approximately 14 dB, the obtained throughput with R = 8/9 becomes lower according to the increase in the N_{Tx} and N_{Rx} values due to the degradation in the signal detection. It is observed, however, that when the average received total E_b/N_0 is greater than approximately 14 dB, where the influence of additive noise is low, the measured throughput is increased according to the increase in the combination of (N_{Tx}, N_{Rx}). Thus, using the QRM-MLD with ASESS, the throughput values of approximately 400 Mbps, 700 Mbps, and 1 Gbps are achieved by 2-by-2, 3-by-3, and 4-by-4 MIMO multiplexing at the average received E_b/N_0 of 17.8, 18.0 and 18.0 dB with R = 8/9, respectively.

E. Effect of Modulation and Coding Schemes (MCSs)

Finally, Fig. 14 shows the measured throughput performance as a function of the average received E_b/N_0 assuming $N_{Tx} = N_{Rx} = 4$ for various modulation and coding scheme combinations. We used MCSs such as {QPSK, R = 1/2}, {QPSK, R = 2/3}, {QPSK, R = 6/7}, {16QAM, R = 1/2}, {16QAM, R = 2/3}, {16QAM, R = 3/4}, and {16QAM, R = 8/9}. The figure shows that according to the increase in the data modulation level and coding rate, although the loss in the required average received E_b/N_0 of the experiments from the simulations is increased, it is suppressed to within 2 dB even with 16QAM and R = 8/9. We conclude that by using the QRM-MLD with ASESS in the 4-by-4 MIMO multiplexing, the throughput values of 500 Mbps, 800 Mbps, and 1 Gbps are achieved at the average received E_b/N_0 of approximately 6.8, 8.9, and 12.0 dB employing {16QAM, R = 1/2}, {16QAM, R = 3/4}, and {16QAM, R = 8/9}, respectively, in the real-time hardware implementation.

VI. Conclusion

This paper presented experimental results on real-time packet transmission of greater than 1 Gbps by 4-by-4 MIMO multiplexing using MLD with a decreased computational complexity level in OFDM radio access. We applied our original algorithm called ASESS in QRM-MLD to reduce the extremely high level of computational complexity in the conventional MLD. We clarified the following results through laboratory experiments employing the implemented real-time MIMO transceiver.

- The experimental results using multipath fading simulators are in good agreement with the computer simulation results in regard to the degradation in the required average received E_b/N_0 of 1-2 dB. This confirms the effectiveness of our original signal detection algorithm, channel estimation filter, and likelihood function generation for successive soft-decision Turbo decoding.
- The clipping effect by the A/D converters mitigated the LLR calculation error in the simulation such that both bits "1" and "-1" do not exist among the remaining symbol replica candidates in the last stage for the QRM-MLD, providing clear improvements in the achievable PER performance.
- Using the QRM-MLD with ASESS, the throughput values of approximately 400 Mbps, 700 Mbps, and 1 Gbps were achieved using 2-by-2, 3-by-3, and 4-by-4 MIMO multiplexing at the average received total E_b/N_0 of 17.8, 18.0 and 18.0 dB for 16QAM modulation with R = 8/9, respectively.
- Finally, by using the QRM-MLD with ASESS in the 4-by-4 MIMO multiplexing, the throughput values of 500 Mbps, 800 Mbps, and 1 Gbps were achieved at the average received E_b/N_0 of approximately 6.8, 8.9, and 12.0 dB employing {16QAM, R = 1/2}, {16QAM, R = 3/4}, and {16QAM, R = 8/9}, respectively, in the real-time hardware implementation.

In conclusion, we showed the feasibility of high-speed real-time packet transmission of greater than 1 Gbps in a 100-MHz channel bandwidth (i.e., 10 bits/second/Hz) by taking advantage of MIMO multiplexing.

References

[1] Recommendation ITU-R M.1645.
[2] H. Atarashi, S. Abeta, and M. Sawahashi, "Variable spreading factor orthogonal frequency and code division multiplexing (VSF-OFCDM) for broadband packet wireless access," IEICE Trans. Commun., vol. E86-B, no. 1, pp. 291-299, Jan. 2003.
[3] Y. Kishiyama, N. Maeda, K. Higuchi, H. Atarashi, and M. Sawahashi, "Transmission Performance Analysis of VSF-OFCDM Broadband Packet Wireless Access Based on Field Experiments in 100-MHz Forward Link," in Proc. IEEE VTC2004-Fall, Sept. 2004.
[4] G. J. Foschini, Jr., "Layered space-time architecture for wireless communication in a fading environment when using multi-element antennas," Bell Labs Tech. J., pp. 41-59, Autumn 1996.
[5] R. D. Murch and K. B. Letaief, "Antenna Systems for Broadband Wireless Access," IEEE Commun. Mag., vol. 40, no. 4, pp. 76-83, April 2002.
[6] A. van Zelst, R. van Nee, and G.A. Awater, "Space division multiplexing (SDM) for OFDM systems," in Proc. IEEE VTC2000-Spring, pp. 1070-1074, May 2000.
[7] P. W. Wolniansky, G. J. Foschini, G. D. Golden, and R. A. Valenzuela, "V-BLAST: an architecture for realizing very high data rates over the rich-scattering wireless channel," in Proc. 1998 URSI International Symposium on Signals, Systems, and Electronics, pp. 295-300, Sep. 1998.
[8] K. Higuchi, H. Kawai, N. Maeda, and M. Sawahashi, "Adaptive Selection of Surviving Symbol Replica Candidates Based on Maximum Reliability in QRM-MLD for OFCDM MIMO Multiplexing," in Proc. IEEE Globecom2004, Nov. 2004.
[9] K. J. Kim and J. Yue, "Joint channel estimation and data detection algorithms for MIMO-OFDM systems," in Proc. Thirty-Sixth Asilomar Conference on Signals, Systems and Computers, pp. 1857-1861, Nov. 2002.
[10] H. Kawai, K. Higuchi, N. Maeda, and M. Sawahashi, "Performance of QRM-MLD employing two-dimensional multi-slot and carrier-averaging channel estimation using orthogonal pilot channel for OFCDM MIMO multiplexing in multipath fading channel," in Proc. Wireless2004, July 2004.
[11] K. Higuchi, H. Kawai, N. Maeda, M. Sawahashi, T. Itoh, Y. Kakura, A. Ushirokawa, and H. Seki, "Likelihood function for QRM-MLD suitable for soft-decision turbo decoding and its performance for OFCDM MIMO multiplexing in multipath fading channel," in Proc. IEEE PIMRC2004, Sept. 2004.